Supporting information

The Manipulation of the Internal Hydrophobicity of FraC Nanopores Augments Peptide Capture and Recognition

Florian Leonardus Rudolfus Lucas[1], Kumar Sarthak[2], Erica Mariska Lenting[1], David Coltan[1], Nieck Jordy van der Heide[1], Roderick Corstiaan Abraham Versloot[1], Aleksei Aksimentiev[2]*, Giovanni Maglia[1]*

[1]*Groningen Biomolecular Sciences and Biotechnology Institute, University of Groningen, 9747 AG Groningen, The Netherlands*
[2] *Department of Physics, University of Illinois at Urbana-Champaign, Urbana, Illinois 61801, United States*

keywords: Protein sequencing, Single-molecule, Mass spectrometry, Proteomics, Nanopores, Nanopore spectrometry

Corresponding Authors
Giovanni Maglia – Email: g.maglia@rug.nl
Aleksei Aksimentiev - Email: aksiment@illinois.edu

Table of Content

Mutation	V (mV)	I_0 (pA)	$\sigma(I_0)$ (pA)	S_0 (nS)	SNR ($I_0/\sigma(I_0)$)	Gating (events·s^{-1})	Median dwell time (µs)
WtFraC-T1	-50 mV	95 ± 1	2.7 ± 0.2	1.92 ± 0.02	35 ± 3	-	90 ± 6
WtFraC-T2	-50 mV	47 ± 3	2.0 ± 0.4	0.93 ± 0.06	22 ± 5	-	101 ± 12
D10G	-50 mV	46 ± 2	2.6 ± 0.3	0.92 ± 0.03	17 ± 2	-	81 ± 2
D10R‡	+50 mV	40 ± 1	2.4 ± 0.2	0.80 ± 0.03	15 ± 5	-	82 ± 23
G13E	-50 mV	89 ± 3	2.7 ± 0.1	1.78 ± 0.05	32 ± 1	-	78 ± 1
G13N	-50 mV	75 ± 4	2.5 ± 0.2	1.49 ± 0.08	30 ± 4	-	100 ± 25
G13H	-50 mV	69 ± 5	2.4 ± 0.2	1.38 ± 0.10	30 ± 3	-	86 ± 8
G13H‡	+50 mV	67 ± 1	3 ± 9	1.39 ± 0.03	23 ± 10	-	78 ± 25
G13V	-50 mV	65 ± 4	12 ± 6	1.31 ± 0.08	5 ± 2	4 ± 2	84 ± 2
G13W	-50 mV	64 ± 8	3.0 ± 0.2	1.29 ± 0.17	21 ± 2	7.3 ± 3.9	321 ± 61
G13F	-50 mV	77 ± 4	2.3 ± 0.2	1.53 ± 0.08	31 ± 4	7.1 ± 0.7	182 ± 29
G13Y	-50 mV	82 ± 3	2.2 ± 0.1	1.63 ± 0.06	36 ± 3	2.3 ± 0.3	219 ± 56
D17K	-50 mV	104 ± 5	2.6 ± 0.2	2.08 ± 0.11	40 ± 5	-	94 ± 7
D17Q	-50 mV	84 ± 3	2.4 ± 0.1	1.68 ± 0.06	36 ± 3	-	80 ± 5
G15T	-50 mV	100 ± 3	2.4 ± 0.5	2.00 ± 0.06	39 ± 6	-	87 ± 8
G15V V22A	-50 mV	113 ± 9	2.9 ± 0.1	2.27 ± 0.19	39 ± 2	-	85 ± 3
K20D	-50 mV	96 ± 10	2.6 ± 0.3	1.91 ± 0.20	38 ± 1	-	101 ± 7
K20D T21K	-50 mV	101 ± 18	2.9 ± 0.2	2.01 ± 0.36	33 ± 5	-	98 ± 9
T21D	-50 mV	101 ± 10	2.6 ± 0.2	2.03 ± 0.20	38 ± 1	-	93 ± 2
K20Q	-50 mV	96 ± 4	2.6 ± 0.1	1.92 ± 0.08	37 ± 2	-	92 ± 13

Supplementary Table 1. Characteristics of Fragaceatoxin C mutant nanopores. The average baseline conductance I_0 is shown with the standard deviation error $\sigma(I_0)$. The average baseline conductance (S_0) is calculated from I_0 and the applied voltage (V). The signal-to-noise ratio (SNR) is calculated by dividing the baseline conductance I_0 by its standard deviation $\sigma(I_0)$. The intrinsic gating of pores is shown for all pores with significant events in the baseline. The median dwell time and standard deviation over 3 independent measurements is shown.

Bias potential (mV)	WtFraC T1	WtFraC T2	D10G	D10R	G13E	G13N	G13H	G13W	G13V	G13F
-150	-297 ± 8	-140 ± 1	-140 ± 12	-106 ± 5	-297 ± 1	-220 ± 23	-191 ± 10	-171 ± 32	-206 ± 5	-176 ± 75
-145	-287 ± 6	-135 ± 1	-150 ± 32	-91 ± 12	-286 ± 1	-213 ± 22	-185 ± 10	-165 ± 32	-199 ± 5	-220 ± 7
-140	-279 ± 7	-130 ± 1	-144 ± 30	-90 ± 9	-275 ± 1	-207 ± 20	-179 ± 9	-94 ± 59	-192 ± 5	-214 ± 7
-135	-269 ± 5	-126 ± 1	-140 ± 28	-87 ± 9	-262 ± 1	-200 ± 20	-173 ± 9	-153 ± 31	-185 ± 5	-160 ± 72
-130	-258 ± 5	-124 ± 1	-134 ± 26	-83 ± 7	-253 ± 1	-193 ± 19	-168 ± 9	-147 ± 31	-179 ± 4	-202 ± 7
-125	-248 ± 4	-117 ± 1	-139 ± 39	-82 ± 8	-242 ± 1	-187 ± 18	-162 ± 9	-141 ± 30	-171 ± 4	-196 ± 7
-120	-239 ± 5	-113 ± 1	-132 ± 35	-77 ± 7	-231 ± 1	-180 ± 16	-156 ± 9	-133 ± 27	-165 ± 4	-130 ± 89
-115	-229 ± 4	-108 ± 1	-117 ± 19	-72 ± 5	-221 ± 1	-173 ± 15	-150 ± 9	-127 ± 26	-157 ± 4	-183 ± 7
-110	-219 ± 4	-104 ± 1	-102 ± 4	-64 ± 10	-210 ± 1	-166 ± 14	-144 ± 8	-121 ± 26	-151 ± 4	-177 ± 7
-105	-209 ± 3	-99 ± 1	-97 ± 3	-64 ± 5	-200 ± 1	-139 ± 41	-138 ± 8	-115 ± 25	-143 ± 3	-170 ± 7
-100	**-199 ± 3**	**-98 ± 1**	**-104 ± 19**	**-59 ± 7**	**-189 ± 2**	**-152 ± 12**	**-132 ± 8**	**-110 ± 24**	**-136 ± 3**	**-116 ± 72**
-95	-189 ± 3	-90 ± 1	-87 ± 2	-58 ± 3	-178 ± 2	-144 ± 11	-126 ± 8	-104 ± 24	-129 ± 3	-109 ± 71
-90	-178 ± 2	-86 ± 1	-83 ± 2	-56 ± 4	-168 ± 1	-137 ± 10	-120 ± 7	-99 ± 25	-122 ± 3	-106 ± 68
-85	-168 ± 2	-82 ± 1	-78 ± 2	-52 ± 5	-158 ± 2	-130 ± 9	-114 ± 7	-93 ± 22	-114 ± 3	-142 ± 8
-80	-158 ± 2	-77 ± 1	-73 ± 2	-47 ± 6	-148 ± 2	-122 ± 8	-107 ± 8	-87 ± 21	-107 ± 2	-133 ± 7
-75	-147 ± 2	-72 ± 1	-69 ± 1	-48 ± 2	-137 ± 2	-114 ± 7	-101 ± 6	-81 ± 20	-100 ± 2	-125 ± 7
-70	-137 ± 1	-68 ± 1	-64 ± 1	-44 ± 2	-127 ± 2	-106 ± 6	-95 ± 6	-76 ± 19	-93 ± 2	-118 ± 7
-65	-127 ± 1	-63 ± 1	-60 ± 1	-41 ± 1	-117 ± 2	-98 ± 6	-88 ± 6	-70 ± 17	-85 ± 2	-110 ± 6
-60	-116 ± 1	-58 ± 1	-55 ± 1	-39 ± 1	-107 ± 2	-91 ± 5	-82 ± 5	-64 ± 16	-78 ± 1	-102 ± 6
-55	-106 ± 1	-53 ± 1	-50 ± 1	-35 ± 1	-97 ± 2	-82 ± 5	-76 ± 5	-59 ± 15	-71 ± 1	-65 ± 44
-50	**-96 ± 1**	**-48 ± 1**	**-46 ± 1**	**-32 ± 1**	**-88 ± 2**	**-74 ± 4**	**-69 ± 5**	**-54 ± 14**	**-63 ± 1**	**-85 ± 5**
-45	-85 ± 1	-43 ± 1	-41 ± 1	-27 ± 4	-78 ± 2	-66 ± 3	-62 ± 4	-48 ± 13	-56 ± 1	-77 ± 5
-40	-75 ± 1	-38 ± 1	-36 ± 1	-21 ± 9	-68 ± 2	-59 ± 2	-55 ± 4	-43 ± 11	-49 ± 1	-68 ± 5
-35	-65 ± 1	-33 ± 1	-32 ± 1	-21 ± 4	-59 ± 2	-51 ± 2	-49 ± 3	-37 ± 10	-43 ± 1	-59 ± 4
-30	-55 ± 1	-28 ± 1	-27 ± 1	-15 ± 7	-50 ± 2	-43 ± 1	-42 ± 3	-32 ± 8	-36 ± 1	-51 ± 4
-25	-45 ± 1	-23 ± 1	-23 ± 1	-12 ± 6	-41 ± 2	-36 ± 1	-35 ± 2	-26 ± 7	-29 ± 1	-42 ± 3
-20	-36 ± 1	-18 ± 1	-18 ± 1	-9 ± 5	-32 ± 1	-28 ± 1	-28 ± 2	-21 ± 5	-23 ± 1	-23 ± 15
-15	-26 ± 1	-14 ± 1	-13 ± 1	-7 ± 4	-24 ± 1	-21 ± 1	-21 ± 1	-16 ± 4	-17 ± 1	-11 ± 12
-10	-17 ± 1	-9 ± 1	-9 ± 1	-4 ± 2	-15 ± 1	-13 ± 1	-14 ± 1	-10 ± 2	-11 ± 1	-16 ± 2
-5	-8 ± 1	-4 ± 1	-4 ± 1	-2 ± 1	-7 ± 1	-6 ± 1	-6 ± 1	-5 ± 1	-5 ± 1	-7 ± 1
0	0 ± 1	0 ± 1	0 ± 1	0 ± 1	0 ± 1	0 ± 1	0 ± 1	0 ± 1	0 ± 1	0 ± 1
5	8 ± 1	4 ± 1	4 ± 1	2 ± 1	8 ± 1	6 ± 1	7 ± 1	5 ± 2	5 ± 1	8 ± 1
10	17 ± 1	9 ± 1	8 ± 1	5 ± 2	15 ± 1	12 ± 1	14 ± 1	10 ± 4	10 ± 1	16 ± 1
15	25 ± 1	13 ± 1	13 ± 1	7 ± 4	23 ± 1	19 ± 1	21 ± 2	15 ± 6	15 ± 1	17 ± 8
20	33 ± 1	17 ± 1	17 ± 1	14 ± 1	30 ± 1	25 ± 1	29 ± 3	21 ± 8	20 ± 1	22 ± 13
25	41 ± 1	21 ± 1	21 ± 1	18 ± 1	37 ± 1	29 ± 2	36 ± 3	26 ± 10	25 ± 1	16 ± 22
30	48 ± 1	25 ± 1	26 ± 1	21 ± 1	44 ± 1	36 ± 1	44 ± 4	31 ± 11	29 ± 1	36 ± 25
35	56 ± 1	29 ± 1	30 ± 1	26 ± 1	51 ± 2	40 ± 3	51 ± 5	37 ± 13	34 ± 1	42 ± 30
40	63 ± 2	33 ± 1	35 ± 1	30 ± 1	57 ± 2	47 ± 2	59 ± 6	42 ± 15	38 ± 1	47 ± 31
45	71 ± 2	37 ± 1	39 ± 2	34 ± 1	64 ± 3	52 ± 2	66 ± 6	47 ± 17	42 ± 1	22 ± 8
50	**78 ± 2**	**40 ± 1**	**44 ± 2**	**39 ± 1**	**71 ± 3**	**53 ± 7**	**74 ± 7**	**52 ± 19**	**46 ± 1**	**60 ± 40**
55	85 ± 2	44 ± 1	48 ± 2	44 ± 1	77 ± 4	59 ± 6	82 ± 8	57 ± 22	50 ± 1	44 ± 30
60	92 ± 2	47 ± 1	52 ± 3	48 ± 2	83 ± 4	62 ± 8	90 ± 9	46 ± 2	54 ± 1	57 ± 35
65	99 ± 3	50 ± 1	57 ± 3	53 ± 2	89 ± 4	66 ± 10	98 ± 10	50 ± 3	58 ± 1	54 ± 34
70	106 ± 3	54 ± 1	61 ± 3	58 ± 2	94 ± 4	69 ± 13	106 ± 11	54 ± 4	61 ± 1	51 ± 35
75	114 ± 3	57 ± 1	66 ± 4	63 ± 2	101 ± 5	76 ± 10	114 ± 12	57 ± 4	65 ± 1	73 ± 56
80	121 ± 3	61 ± 1	70 ± 4	69 ± 1	108 ± 6	84 ± 6	122 ± 12	61 ± 5	69 ± 1	26 ± 10
85	128 ± 3	64 ± 1	75 ± 4	74 ± 1	114 ± 6	79 ± 18	131 ± 13	65 ± 5	72 ± 1	61 ± 76
90	135 ± 4	67 ± 1	80 ± 4	79 ± 2	120 ± 7	90 ± 10	140 ± 14	68 ± 4	76 ± 1	70 ± 77
95	142 ± 4	70 ± 1	84 ± 5	84 ± 2	127 ± 7	87 ± 20	149 ± 15	71 ± 5	79 ± 1	82 ± 83
100	**149 ± 4**	**74 ± 1**	**89 ± 5**	**89 ± 2**	**131 ± 8**	**90 ± 21**	**158 ± 16**	**77 ± 8**	**82 ± 1**	**122 ± 93**
105	157 ± 4	77 ± 1	93 ± 5	95 ± 2	139 ± 8	93 ± 25	167 ± 17	80 ± 9	87 ± 1	148 ± 85
110	164 ± 4	81 ± 1	98 ± 5	100 ± 2	145 ± 8	97 ± 26	176 ± 18	82 ± 7	91 ± 1	140 ± 63
115	172 ± 4	83 ± 1	103 ± 5	106 ± 2	152 ± 9	103 ± 25	186 ± 18	88 ± 11	94 ± 1	152 ± 51
120	179 ± 4	87 ± 1	82 ± 42	112 ± 2	105 ± 67	109 ± 24	195 ± 20	92 ± 12	98 ± 1	127 ± 93
125	144 ± 58	91 ± 1	84 ± 46	117 ± 2	166 ± 10	113 ± 25	206 ± 20	92 ± 9	102 ± 1	106 ± 95
130	193 ± 5	94 ± 1	88 ± 47	86 ± 49	172 ± 10	115 ± 30	216 ± 21	71 ± 41	106 ± 1	151 ± 50
135	155 ± 64	96 ± 1	92 ± 49	129 ± 3	180 ± 10	121 ± 29	227 ± 22	77 ± 39	110 ± 1	173 ± 63
140	211 ± 5	102 ± 1	96 ± 51	135 ± 3	187 ± 11	125 ± 31	238 ± 23	142 ± 64	115 ± 1	106 ± 67
145	219 ± 5	105 ± 1	100 ± 53	140 ± 3	194 ± 11	129 ± 33	249 ± 24	110 ± 15	118 ± 1	128 ± 62
150	228 ± 6	109 ± 1	104 ± 55	147 ± 3	200 ± 12	134 ± 35	260 ± 25	113 ± 16	93 ± 43	108 ± 79

Supplementary Table 2A. Voltage-current (IV) curves of Fragaceatoxin C mutants. Current (pA) at different applied bias potentials (mV) for Fragaceatoxin C mutants measured in 1 M KCl, 50 mM citric acid (pH 3.8).

Bias potential (mV)	G13Y	G15T	D17K	D17Q	K20D	T21D	K20Q	K20D T21K	G15V V22A
-150	-218 ± 31	-312 ± 18	-162 ± 4	-260 ± 12	-396 ± 24	-339 ± 8	-332 ± 78	-337 ± 6	-300 ± 4
-145	-211 ± 31	-302 ± 17	-159 ± 4	-252 ± 9	-382 ± 24	-327 ± 8	-320 ± 76	-325 ± 6	-291 ± 4
-140	-204 ± 31	-292 ± 17	-158 ± 4	-246 ± 8	-256 ± 96	-314 ± 7	-308 ± 73	-314 ± 5	-281 ± 3
-135	-197 ± 32	-283 ± 16	-154 ± 4	-239 ± 6	-354 ± 22	-302 ± 7	-298 ± 69	-302 ± 5	-271 ± 3
-130	-197 ± 37	-273 ± 15	-152 ± 4	-232 ± 5	-341 ± 22	-290 ± 6	-290 ± 61	-291 ± 5	-261 ± 2
-125	-183 ± 31	-263 ± 15	-149 ± 4	-226 ± 3	-326 ± 20	-278 ± 6	-277 ± 59	-279 ± 5	-251 ± 2
-120	-175 ± 32	-253 ± 14	-146 ± 4	-218 ± 1	-313 ± 21	-266 ± 5	-262 ± 61	-268 ± 5	-241 ± 2
-115	-168 ± 31	-242 ± 13	-143 ± 4	-211 ± 1	-300 ± 21	-254 ± 5	-252 ± 56	-257 ± 5	-231 ± 1
-110	-160 ± 31	-232 ± 13	-140 ± 4	-203 ± 1	-283 ± 19	-243 ± 5	-240 ± 54	-245 ± 5	-221 ± 1
-105	-153 ± 31	-222 ± 12	-137 ± 4	-195 ± 1	-269 ± 17	-231 ± 4	-231 ± 48	-234 ± 5	-211 ± 1
-100	**-145 ± 31**	**-212 ± 12**	**-133 ± 4**	**-188 ± 1**	**-259 ± 16**	**-219 ± 3**	**-217 ± 47**	**-223 ± 4**	**-158 ± 59**
-95	-138 ± 31	-201 ± 11	-129 ± 3	-180 ± 2	-241 ± 16	-207 ± 3	-205 ± 44	-211 ± 4	-190 ± 1
-90	-130 ± 30	-191 ± 10	-126 ± 3	-171 ± 3	-227 ± 16	-196 ± 2	-193 ± 41	-199 ± 4	-180 ± 1
-85	-122 ± 30	-180 ± 10	-121 ± 3	-163 ± 3	-212 ± 15	-184 ± 2	-182 ± 37	-188 ± 4	-170 ± 1
-80	-114 ± 29	-170 ± 9	-117 ± 3	-154 ± 3	-198 ± 14	-172 ± 2	-169 ± 35	-177 ± 3	-159 ± 2
-75	-106 ± 28	-159 ± 9	-112 ± 3	-146 ± 3	-185 ± 12	-160 ± 1	-158 ± 32	-165 ± 3	-149 ± 2
-70	-98 ± 27	-148 ± 8	-107 ± 3	-137 ± 3	-170 ± 12	-149 ± 1	-146 ± 29	-154 ± 3	-138 ± 2
-65	-90 ± 25	-137 ± 8	-102 ± 2	-128 ± 3	-156 ± 12	-137 ± 1	-134 ± 26	-142 ± 3	-128 ± 2
-60	-82 ± 24	-126 ± 7	-96 ± 2	-118 ± 3	-143 ± 11	-125 ± 1	-122 ± 23	-131 ± 3	-117 ± 2
-55	-75 ± 22	-115 ± 6	-90 ± 2	-109 ± 3	-129 ± 10	-114 ± 1	-111 ± 20	-119 ± 2	-107 ± 2
-50	**-67 ± 20**	**-104 ± 6**	**-83 ± 2**	**-99 ± 3**	**-116 ± 9**	**-103 ± 1**	**-100 ± 17**	**-108 ± 2**	**-96 ± 3**
-45	-56 ± 17	-93 ± 5	-76 ± 2	-90 ± 2	-103 ± 8	-91 ± 1	-88 ± 15	-97 ± 2	-86 ± 3
-40	-43 ± 17	-83 ± 5	-69 ± 2	-80 ± 2	-90 ± 7	-80 ± 1	-77 ± 13	-85 ± 2	-76 ± 3
-35	-44 ± 14	-72 ± 4	-62 ± 2	-70 ± 1	-77 ± 7	-69 ± 1	-67 ± 11	-74 ± 1	-66 ± 3
-30	-23 ± 19	-61 ± 3	-54 ± 1	-60 ± 1	-65 ± 5	-59 ± 1	-56 ± 9	-63 ± 1	-56 ± 2
-25	-20 ± 16	-50 ± 3	-46 ± 1	-50 ± 1	-53 ± 4	-48 ± 1	-46 ± 7	-52 ± 1	-46 ± 2
-20	-16 ± 12	-40 ± 2	-37 ± 1	-40 ± 1	-42 ± 4	-38 ± 1	-36 ± 5	-41 ± 1	-36 ± 2
-15	-11 ± 9	-30 ± 2	-28 ± 1	-30 ± 1	-31 ± 3	-28 ± 1	-26 ± 4	-31 ± 1	-26 ± 1
-10	-7 ± 6	-19 ± 1	-19 ± 1	-20 ± 1	-20 ± 2	-18 ± 1	-17 ± 2	-20 ± 1	-17 ± 1
-5	-2 ± 3	-9 ± 1	-9 ± 1	-10 ± 1	-9 ± 1	-9 ± 1	-8 ± 1	-10 ± 1	-8 ± 1
0	1 ± 1	0 ± 1	0 ± 1	0 ± 1	0 ± 1	0 ± 1	0 ± 1	0 ± 1	0 ± 1
5	5 ± 2	9 ± 1	10 ± 1	9 ± 1	9 ± 1	9 ± 1	8 ± 1	9 ± 1	9 ± 1
10	4 ± 3	19 ± 1	20 ± 1	19 ± 1	18 ± 1	17 ± 1	16 ± 1	19 ± 1	17 ± 1
15	5 ± 4	28 ± 2	31 ± 2	29 ± 1	27 ± 2	26 ± 1	24 ± 2	29 ± 1	25 ± 2
20	7 ± 6	37 ± 2	42 ± 2	39 ± 1	35 ± 3	34 ± 1	31 ± 3	38 ± 1	33 ± 2
25	9 ± 8	46 ± 3	53 ± 3	49 ± 1	43 ± 4	42 ± 1	38 ± 3	47 ± 1	41 ± 3
30	10 ± 9	55 ± 4	64 ± 4	58 ± 1	51 ± 5	50 ± 2	45 ± 4	56 ± 1	49 ± 4
35	12 ± 10	63 ± 5	76 ± 5	68 ± 1	59 ± 6	57 ± 2	52 ± 4	65 ± 1	56 ± 4
40	12 ± 11	72 ± 5	88 ± 6	77 ± 1	65 ± 7	64 ± 3	58 ± 5	73 ± 1	64 ± 5
45	15 ± 12	80 ± 6	98 ± 9	86 ± 1	72 ± 8	71 ± 3	64 ± 5	82 ± 1	71 ± 6
50	**18 ± 13**	**89 ± 7**	**112 ± 8**	**95 ± 1**	**79 ± 9**	**78 ± 4**	**70 ± 6**	**90 ± 2**	**78 ± 7**
55	19 ± 15	97 ± 7	124 ± 9	104 ± 1	86 ± 9	85 ± 4	76 ± 6	98 ± 3	86 ± 8
60	19 ± 17	105 ± 8	136 ± 10	113 ± 2	92 ± 10	92 ± 5	82 ± 6	106 ± 3	93 ± 8
65	20 ± 21	113 ± 9	149 ± 11	122 ± 2	98 ± 11	99 ± 5	87 ± 7	113 ± 4	99 ± 9
70	24 ± 20	121 ± 9	162 ± 13	131 ± 2	104 ± 12	105 ± 6	93 ± 7	121 ± 5	106 ± 10
75	24 ± 19	129 ± 10	99 ± 40	139 ± 2	109 ± 13	112 ± 6	99 ± 7	128 ± 6	113 ± 11
80	20 ± 12	137 ± 11	142 ± 57	147 ± 3	116 ± 13	118 ± 7	104 ± 8	135 ± 7	120 ± 12
85	32 ± 25	145 ± 11	150 ± 62	155 ± 3	121 ± 14	125 ± 8	109 ± 8	143 ± 8	127 ± 13
90	32 ± 24	153 ± 12	161 ± 65	164 ± 4	128 ± 15	132 ± 8	114 ± 9	150 ± 9	134 ± 14
95	37 ± 29	161 ± 12	172 ± 68	172 ± 5	133 ± 16	138 ± 8	119 ± 10	157 ± 10	142 ± 14
100	**33 ± 28**	**169 ± 13**	**181 ± 70**	**180 ± 7**	**137 ± 15**	**145 ± 9**	**124 ± 11**	**164 ± 11**	**149 ± 15**
105	29 ± 20	177 ± 14	214 ± 53	188 ± 8	143 ± 15	151 ± 9	129 ± 11	171 ± 12	156 ± 15
110	33 ± 24	185 ± 15	203 ± 81	196 ± 9	147 ± 15	158 ± 10	134 ± 12	178 ± 14	163 ± 15
115	41 ± 35	194 ± 15	283 ± 24	204 ± 11	154 ± 16	166 ± 10	136 ± 12	185 ± 15	172 ± 15
120	22 ± 10	203 ± 15	298 ± 26	211 ± 12	157 ± 15	173 ± 11	144 ± 13	195 ± 16	180 ± 16
125	40 ± 33	211 ± 16	312 ± 28	218 ± 14	164 ± 18	180 ± 11	149 ± 14	200 ± 18	188 ± 18
130	44 ± 37	220 ± 16	328 ± 29	227 ± 16	169 ± 18	181 ± 5	154 ± 15	206 ± 20	196 ± 18
135	48 ± 41	229 ± 17	343 ± 31	235 ± 19	171 ± 16	194 ± 12	159 ± 16	214 ± 21	204 ± 19
140	45 ± 35	239 ± 19	358 ± 32	243 ± 21	173 ± 13	201 ± 12	164 ± 17	222 ± 23	212 ± 20
145	56 ± 43	245 ± 16	373 ± 33	251 ± 23	178 ± 13	209 ± 13	169 ± 18	222 ± 30	220 ± 20
150	59 ± 41	256 ± 18	389 ± 34	258 ± 26	192 ± 22	217 ± 13	172 ± 22	230 ± 33	174 ± 88

Supplementary Table 2B. Voltage-current (IV) curves of Fragaceatoxin C mutants. Current (pA) at different applied bias potentials (mV) for Fragaceatoxin C mutants measured in 1 M KCl, 50 mM citric acid (pH 3.8).

Sequence	Molecular weight (Da)	Charge at pH 3.8
NLCNIPCSALLSSDITASVNCAK	2336.12	+ 1.0
IVSDGNGMNAW	1162.51	0.0
GILQINSR	899.52	+ 1.2
NTDGSTDY	871.32	- 0.2
CELAAAMK	835.40	+ 1.0
NTQATNR	803.39	+ 1.2
GTDVQAW	775.35	0.0
HGLDNY	717.31	+1.0
SLGNW	575.27	+ 0.2
CNDGR	563.21	+ 1.0
TPGSR	516.27	+ 1.2

Supplementary Table 3. Lysozyme peptides resulting from a non-specific trypsin/chymotrypsin digest.

Peptide sequence	Molecular weight (Da)	*m/z*	Charge	Relative abundance (%)	PTM
NLC(+57.02)NIPC(+57.02)SALLSSDITASVNC(+57.02)AK	2507.182	1254.602	2	100	Carbamidomethylation
FESNFNTQATNR	1427.643	714.8295	2	85.8	
GILQINSR	899.5189	450.7684	2	79.8	
KIVSDGDGMNAW	1291.587	646.803	2	66.2	
WWC(+57.02)NDGR	992.3923	497.2051	2	65.3	Carbamidomethylation
NLC(+57.02)NIPC(+57.02)SALL	1273.616	637.8157	2	59.8	Carbamidomethylation
SLGNWVC(+57.02)AAK	1104.539	553.2784	2	59.1	Carbamidomethylation
SSDITASVNC(+57.02)AK	1251.577	626.7985	2	55.1	Carbamidomethylation
IVSDGDGMNAW	1163.492	582.7549	2	49.6	
NLC(+57.02)NIPC(+57.02)SALLSSDITASVN	2148.019	1075.021	2	37.1	Carbamidomethylation
LSSDITASVNC(+57.02)AK	1364.661	683.3383	2	34	Carbamidomethylation
NTDGSTDYGILQINSR	1752.828	877.4232	2	30.6	
FESN(+.98)FNTQATNR	1428.627	715.3217	2	30.3	Deamidation
SALLSSDITASVNC(+57.02)AK	1635.814	818.9156	2	29.1	Carbamidomethylation
NLC(+57.02)N(+.98)IPC(+57.02)SALLSSDITASVNC(+57.02)AK	2508.166	1255.093	2	28.1	Carbamidomethylation Deamidation
NLC(+57.02)NIPC(+57.02)SALLSSDITASVN(+.98)C(+57.02)AK	2508.166	1255.094	2	27.8	Carbamidomethylation Deamidation
YC(+57.02)AIVSAGQ(+.98)N(+.98)ALHFSSGSLDLLAK	2523.231	842.0687	3	27	Carbamidomethylation Deamidation
AAALAGINSR	942.5247	472.2708	2	26.7	
N(+.98)LC(+57.02)NIPC(+57.02)SALLSSDITASVNC(+57.02)AK	2508.166	1255.093	2	26.6	Deamidation Carbamidomethylation
KIVSDGDGM(+15.99)NAW	1307.582	654.799	2	26.3	Oxidation
HGLDNYRGY	1093.494	547.7551	2	25.1	
ESNFNTQATNR	1280.575	641.2963	2	23.9	
SSDITASVN(+.98)C(+57.02)AK	1252.561	627.2888	2	23.6	Deamidation Carbamidomethylation
SLGN(+.98)WVC(+57.02)AAK	1105.523	553.7689	2	23.2	Deamidation Carbamidomethylation
LGEDNINVVEGNEQF	1675.769	838.8934	2	23.2	
NLC(+57.02)NIPC(+57.02)SAL	1160.532	581.2738	2	23.1	Carbamidomethylation
NTDGSTDYGILQIN(+.98)SR	1753.812	877.9144	2	22.6	Deamidation
HGLDN(+.98)YR	874.3933	438.2048	2	21	Deamidation
WWC(+57.02)N(+.98)DGR	993.3763	497.6954	2	21	Carbamidomethylation Deamidation
SSDITASVNC(+57.02)AKK	1379.672	690.8423	2	20.8	Carbamidomethylation
KFESNFNTQATNR	1555.738	778.8769	2	20.7	
SSGTSYPDVLK	1152.566	577.2905	2	20.4	
IVSDGDGM(+15.99)NAW	1179.487	590.7489	2	20.2	Oxidation
KIVSDGNGMNAW	1290.603	646.3096	2	17.3	
LGEDNINVVEGNEQFISASK	2162.049	721.6898	3	16.8	
GRC(+57.02)ELAAAMK	1105.537	553.7755	2	14.5	Carbamidomethylation
STALAN(+.98)QAAM	977.4488	489.7285	2	14.3	Deamidation
NTDGSTDYGILQI	1395.652	698.833	2	13.6	
NTDGSTDYGIL	1154.509	578.2621	2	13.4	
KIVSDGDGMN(+.98)AW	1292.571	647.2928	2	13.3	Deamidation
HGLDN(+.98)YRGY	1094.478	548.2425	2	12.8	Deamidation
GYSLGNWVC(+57.02)AAK	1324.623	663.32	2	12.8	Carbamidomethylation
AAALAGIN(+.98)SR	943.5087	472.7613	2	12.7	Deamidation
RIVSDGDGMNAW	1319.593	660.8039	2	12.3	
SAYPGQITSNMF	1314.591	658.304	2	12.3	
NLC(+57.02)NIPC(+57.02)	889.3786	445.6983	2	11.6	Carbamidomethylation
WWC(+57.02)N(+.98)DGRTPGSR	1491.631	746.823	2	11.4	Carbamidomethylation Deamidation
ESN(+.98)FNTQATNR	1281.559	641.7872	2	11.1	Deamidation
LSSDITASVN(+.98)C(+57.02)AK	1365.645	683.8296	2	10.7	Deamidation Carbamidomethylation
NLC(+57.02)NIPC(+57.02)SALLSSDITASVNC(+57.02)AKK	2635.277	1318.631	2	10.5	Carbamidomethylation
LSGNWIR	844.4555	423.2351	2	10.3	
LLSSDITASVNC(+57.02)AK	1477.745	739.8796	2	10.3	Carbamidomethylation
LC(+57.02)NIPC(+57.02)SALLSSDITASVNC(+57.02)AK	2393.139	1197.579	2	10.2	Carbamidomethylation

Supplementary Table 4. Lysozyme peptides resulting from a non-specific trypsin/chymotrypsin digest as measured by ESI-MS. The peptide sequence is shown, with mass modifications as well as the total mass of the peptide. The charge is calculated from the mass-over-charge ratio (m/z) and the relative abundance is calculated from the base peak (highest intensity). The final column shows the detection post translation modification (PTM). All spectra were analysed using PEAKS Studio and comparison with the *Gallus-Gallus* lysozyme (P00698|LYSC_CHICK) sequence.

	Events·s^{-1} where $\beta > 0$	Events·s^{-1} where $\beta > 1$	Events·s^{-1} where $\beta > 10$
WtFraC-T1	13.5 ± 1.6	13.4 ± 1.6	7.4 ± 1
WtFraC-T2	11.4 ± 2.5	11.2 ± 2.6	7.7 ± 2
D10G	3.8 ± 0.7	3.8 ± 0.6	2.9 ± 0.5
D10R‡	9.9 ± 1.3	9.8 ± 1.3	7.5 ± 0.6
G13E	7.4 ± 0.8	7.1 ± 0.7	3.9 ± 0.4
G13N	17.4 ± 17.2	15.4 ± 15.4	10.5 ± 10.8
G13H	11.7 ± 2.2	11.2 ± 2	7.8 ± 2.1
G13H‡	3.4 ± 0.7	3.3 ± 0.7	2.4 ± 0.8
G13W	43 ± 8.8	41.9 ± 8.7	29.7 ± 7.6
G13V	17.6 ± 0.1	17 ± 0.1	11.6 ± 0.6
G13F	41.3 ± 3.5	40.9 ± 3.5	30.2 ± 1.6
G13Y	43.2 ± 8.1	42.6 ± 7.7	27.3 ± 3.8
D17K	2.8 ± 0.9	2.5 ± 0.8	1.8 ± 0.5
D17Q	1.8 ± 0.5	1.8 ± 0.5	1.2 ± 0.3
G15T	12.5 ± 1.5	12.4 ± 1.5	7.4 ± 0.4
G15V V22A	8.2 ± 0.4	8.1 ± 0.3	4.7 ± 0.5
K20D	18.5 ± 0.4	18 ± 0.3	10.2 ± 0.5
K20D T21K	11.7 ± 0.8	11.2 ± 0.7	6.3 ± 0.4
T21D	9.4 ± 1.6	9.2 ± 1.5	5.1 ± 1
K20Q	24.3 ± 10.9	22.6 ± 8.7	15.4 ± 8.6

Supplementary Table 5. Event rates resulting from the addition of unspecific lysozyme digest to FraC mutants. The event rate is shown for all events β >0, events with β >1, and events with β > 10.

	pH 7.5		**pH 3.8**	
	Reversal potential (mV)	P_{K^+} / P_{Cl^-}	Reversal potential (mV)	P_{K^+} / P_{Cl^-}
WtFraC-T1	17.2 ± 1.2*	3.6 ± 0.4*	1.0 ± 1.7	1.03 ± 0.04
WtFraC-T2	20.8 ± 1.6*	5.2 ± 0.9*	0.7 ± 4.9	1.1 ± 0.4
G13F-FraC-T1	17.0 ± 0.7	3.7 ± 0.2	0.0 ± 0.4	1.00 ± 0.03

*replicated from Huang *et al.* 2019

Supplementary Table 6. Reversal potentials of WtFraC-T1, WtFraC-T2, and G13F-FraC-T1 at pH 7.5 and pH 3.8.

Mutation	Forward Primer
G13E	5'-GGTGCGGAACTGGGCTTTGACGTACTG-3'
G13N	5'-CGGTGCGAATCTGGGCTTTGAC-3'
G13H	5'-GGTGCGCATCTGGGCTTTGACGTAC-3'
G13W	5'-GGTGCGTGGCTGGGCTTTGACGTACTG-3'
G13F	5'-GGTGCGTTCCTGGGCTTTGACGTACTG-3'
G13Y	5'-GGTGCGTATCTGGGCTTTGACGTACTG-3'
G15T	5'-CGGGTCTGACCTTTGACGTACTG-3'
G15V	5'-CGGGTCTGGTCTTTGACGTACTG-3'
D17K	5'-CTGGGCTTTAAGGTACTGAAAACCGTGC-3'
D17Q	5'-CTGGGCTTTCAAGTACTGAAAACCGTGC-3'
D17W	5'-CTGGGCTTTTGGGTACTGAAAACCGTG-3'
G15V V22A	5'-CGGGTCTGGTCTTTGACGTACTG-3'
K20D	5'-CGTACTGGACACCGTGCTGGAG-3'
K20D T21K	5'-GACGTACTGGACAAGGTGCTGGAG-3'
T21D	5'-GTACTGAAAGACGTGCTGGAGGCC-3'
K20Q	5'-CGTACTGCAAACCGTGCTGGAG-3'
G15T K20D	5'-GTACTGGACACCGTGCTGGAG-3'

Supplementary Table 7. Forward primers used in conjunction with T7 reverse (5'-GCTAGTTATTGCTCAGCGG-3') for the mutation of wild-type Fragaceatoxin C

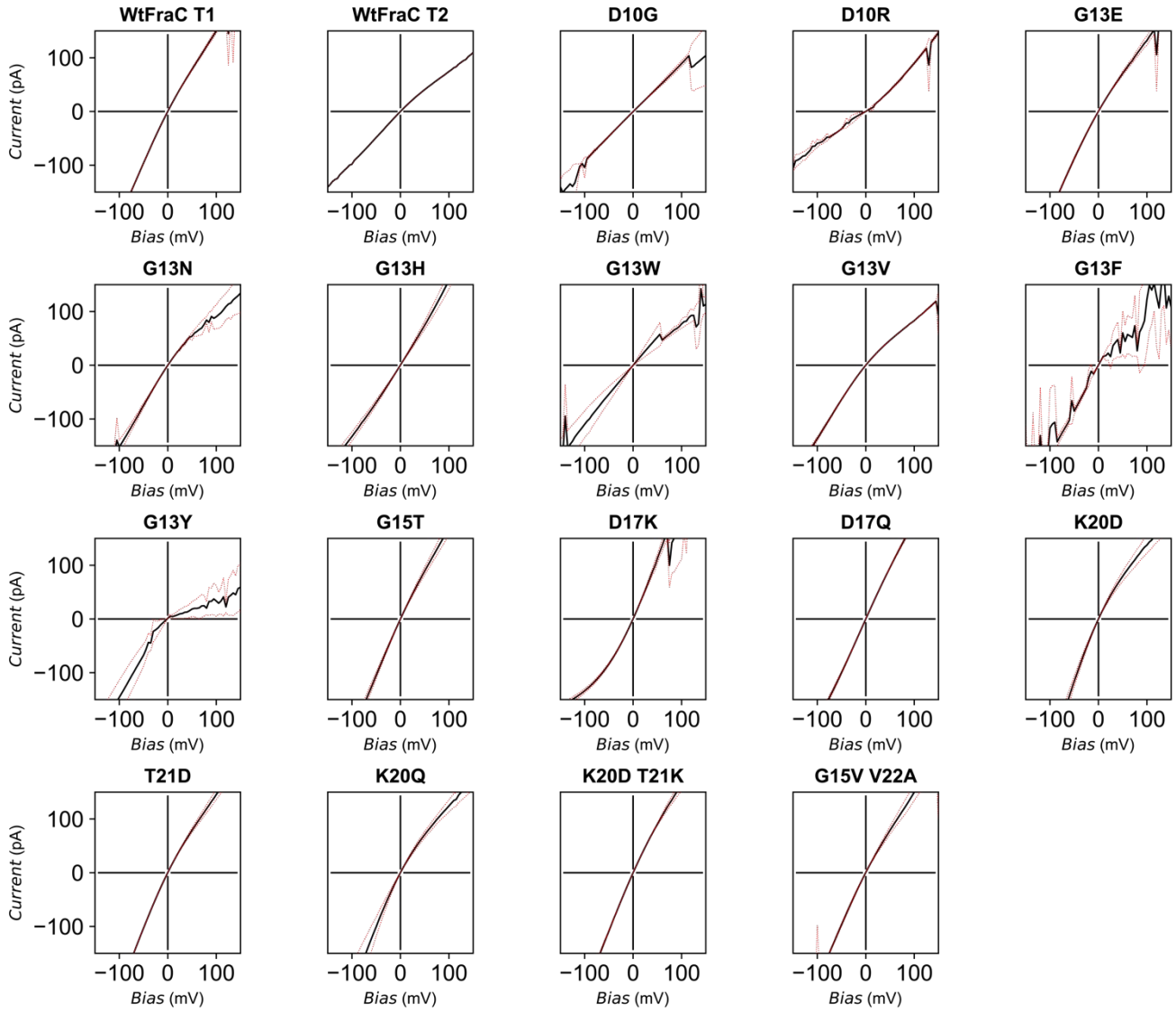

Supplementary figure 1. Voltage-current (IV) curves of Fragaceatoxin C mutants. Current (pA) at different applied bias potentials (mV) for Fragaceatoxin C mutants measured in 1 M KCl, 50 mM citric acid (pH 3.8).

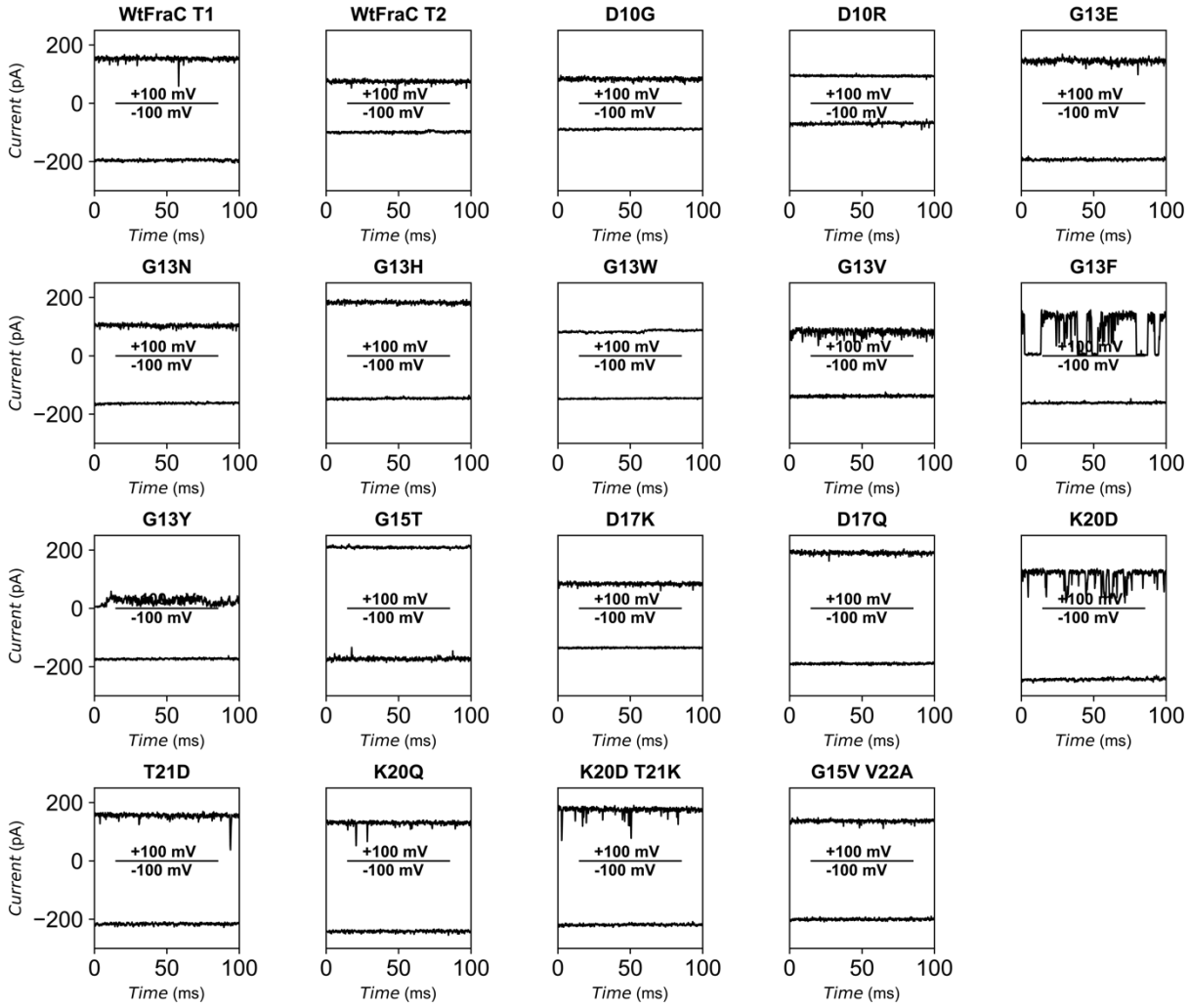

Supplementary figure 2. Baseline current behaviour of Fragaceatoxin C mutants at positive and negatively applied potential. Current (pA) behaviour at an positively applied bias of 100 mV (above middle line) and negatively applied bias of 100 mV (below middle line) for different Fragaceatoxin C mutants. Data was collected in 1 M KCl and 50 mM citric acid titrated with bis-tris propane to pH 3.8 at a sampling frequency of 50 kHz, using a 10 kHz Bessel filter and 5 kHz Gaussian filter.

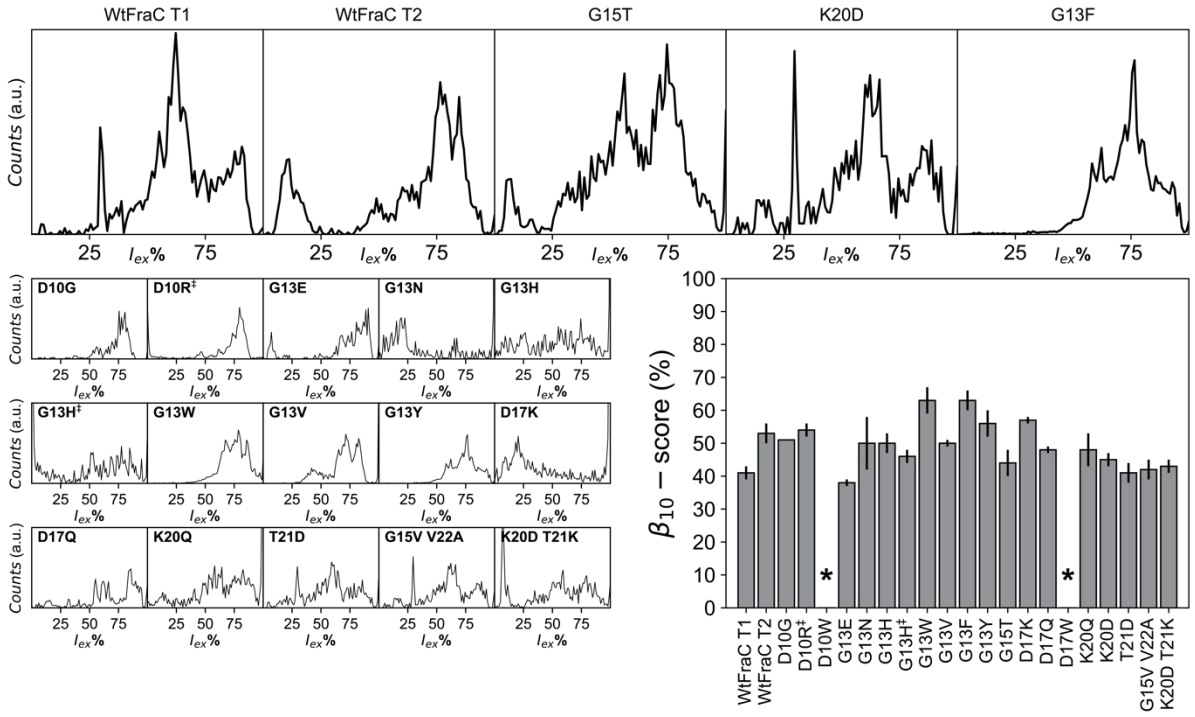

Supplementary figure 3. Residual current histograms of (mutant) Fragaceatoxin C with trypsin digested lysozyme. A: Representative residual current histograms of (mutant) Fragaceatoxin C combined with equal units of trypsin digested lysozyme under an applied potential of -50 mV. **B:** Number of detected events with a β parameter larger than 100 relative to the number of events with a β larger than 1, representing the percentage of well characterizable events relative to the total number of events, for a tryptic digest of lysozyme in multiple Fragaceatoxin C mutants. Data was collected in 1 M KCl and 50 mM citric acid titrated with bis-tris propane to pH 3.8 at a sampling frequency of 50 kHz, using a 10 kHz Bessel filter and 5 kHz Gaussian filter.

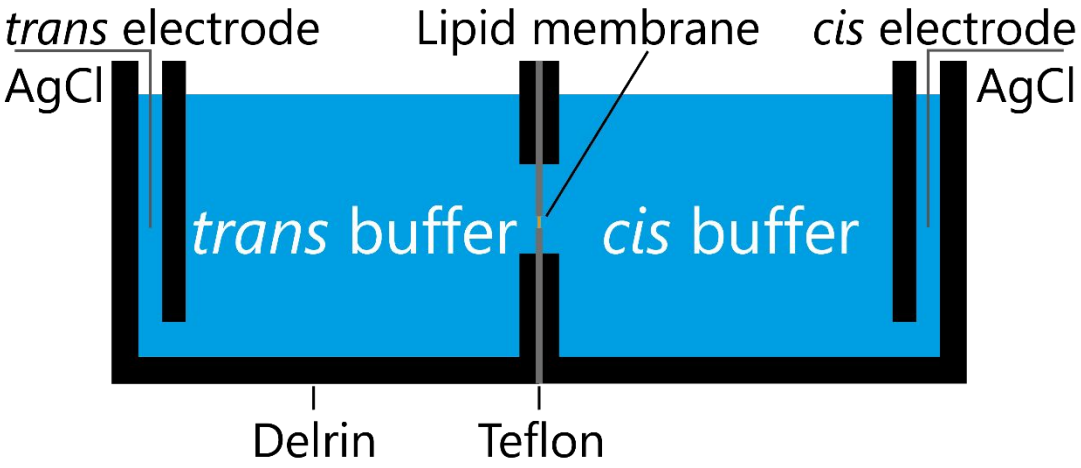

Supplementary figure 4. Electrophysiology setup. The schematic shows a chamber consisting of two compartments made of Delrin, separated by a Teflon film containing a 100 µm hole. Both compartments were filled with buffer and a silver/silver-chloride electrode is attached to serve as a liquid-solid interface for the detector. A lipid membrane is formed over the hole inside the Teflon film using the Langmuir-Blodgett method and nanopore are added to the cis compartment to allow nanopore insertion.

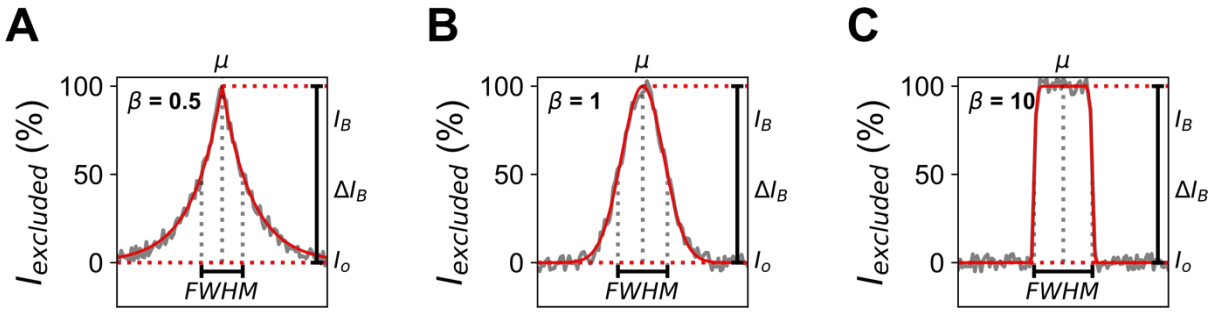

Supplementary figure 5. Effect of the β parameter on the super-Gaussian function shape. Super-Gaussian function shape with μ=0, ΔI_B=100 and σ =1 with in **A:** β = 0.5, **B:** β = 1, **C:** β = 10.

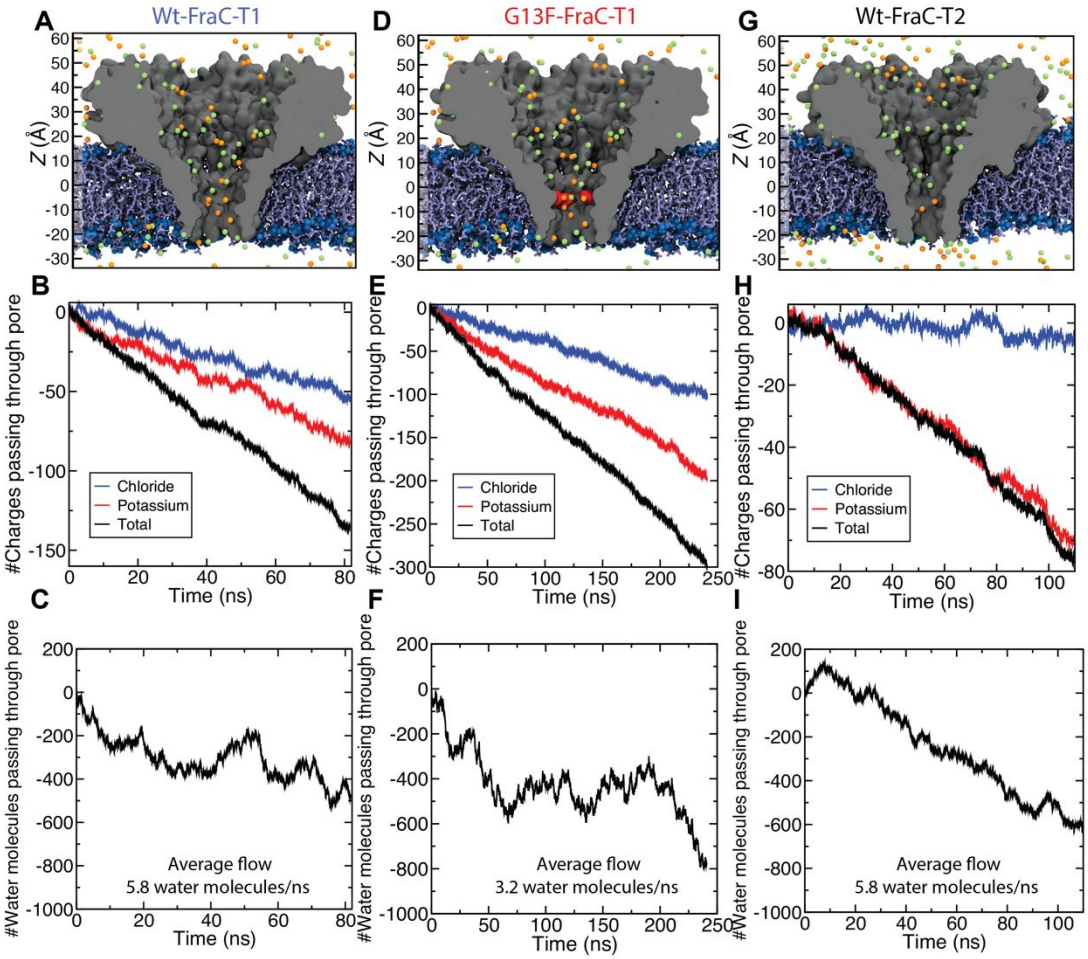

Supplementary Figure 6: MD simulation of ion transport through mutant Fragaceatoxin C nanopores. A: All-atom model of WtFraC-T1 pore. The protein is shown as a gray cutaway surface, embedded in a DPhPC lipid bilayer (blue) and contains 1 M KCl solution (potassium in orange and chloride in green, water not shown). The protonation states of the titratable residues are set to reflect pH of 3.8. The *z* axis is shown on the left for scale. **B:** The charge carried by the chloride (blue) and potassium (red) ions through the pore as a function of the simulation time along with the total charge (black) **C:** The total number of water molecules that pass through the pore constriction as a function of simulation time. The average rate of transport is approximately 5.8 molecules/ns. **,D-F:** Same as A-C but for the G13F-FraC-T1 pore. **G-I**: Same as A-C but for the Wt-FraC-T2 pore.

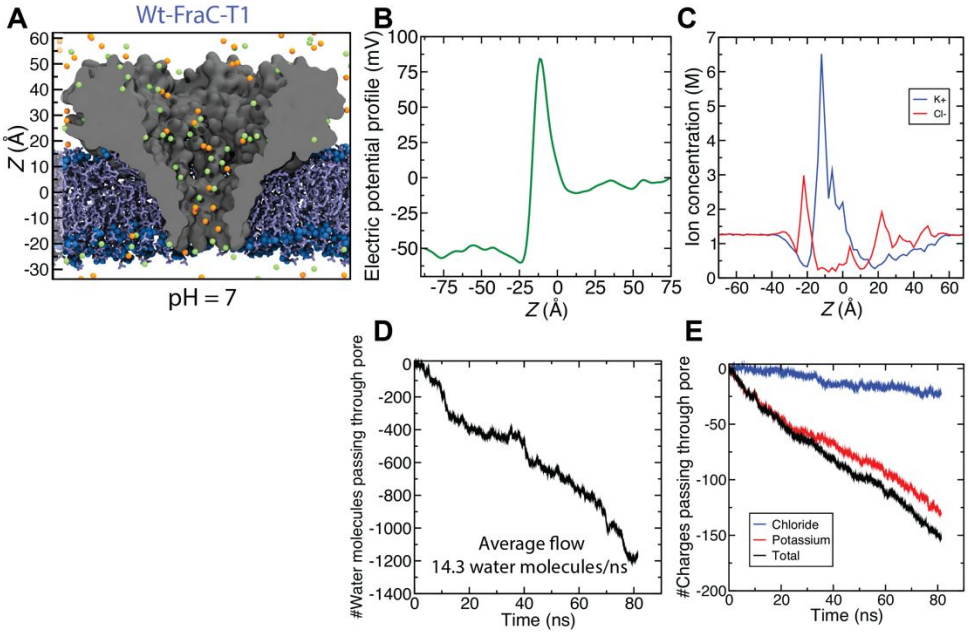

Supplementary Figure 7: Molecular dynamics simulation of Wt-FraC-T1 pore at pH 7. A: All-atom model of WtFraC-T1 pore. The protein is shown as a gray cutaway surface, embedded in a DPhPC lipid bilayer (blue) and contains 1 M KCl solution (potassium in orange and chloride in green, water not shown). The protonation states of the titratable residues are set to reflect pH of 7. The *z* axis is shown on the left for scale. **B:** Average electrostatic potential along the symmetry axis (*z* axis) of the pore, calculated from an 80 ns MD trajectory. **C:** Average local concentration profiles of potassium (blue) and chloride (red) ions along the symmetry axis of the nanopore. **D:** The total number of water molecules that pass through the pore constriction as a function of simulation time. The average rate of transport is approximately 14.3 molecules/ns. **E:** The charge carried by the chloride (blue) and potassium (red) ions through the pore as a function of the simulation time along with the total charge (black). Upon scaling of the raw MD current with the ratio of the experimental and simulated bulk conductivity of 1 M KCl, the average simulated ionic current through Wt-Frac-T1 pore at pH 7 and -50 mV is -187.5 +/- 6.9 pA a factor 1.5 higher than the corresponding experimental value.[21]

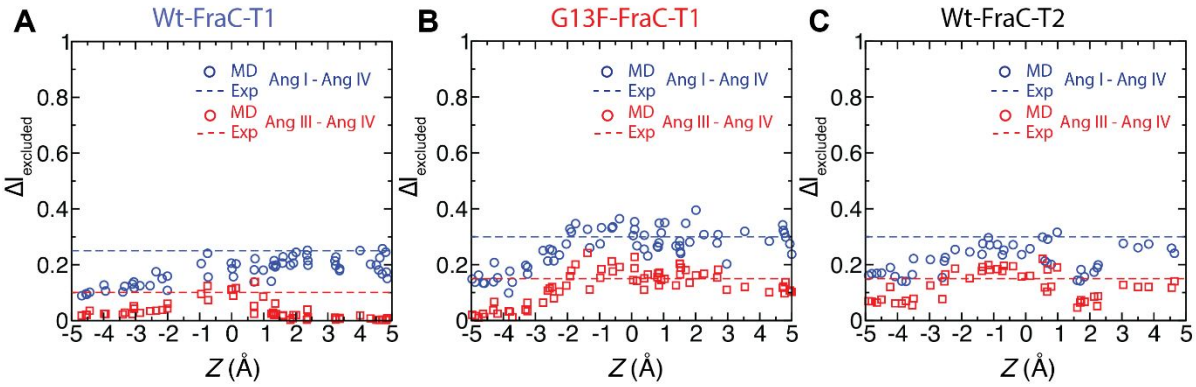

Supplementary Figure 8. Comparison of relative excluded currents in the sensing region. The difference in raw relative excluded current from MD simulation in the sensing region compared to the experimental differences.

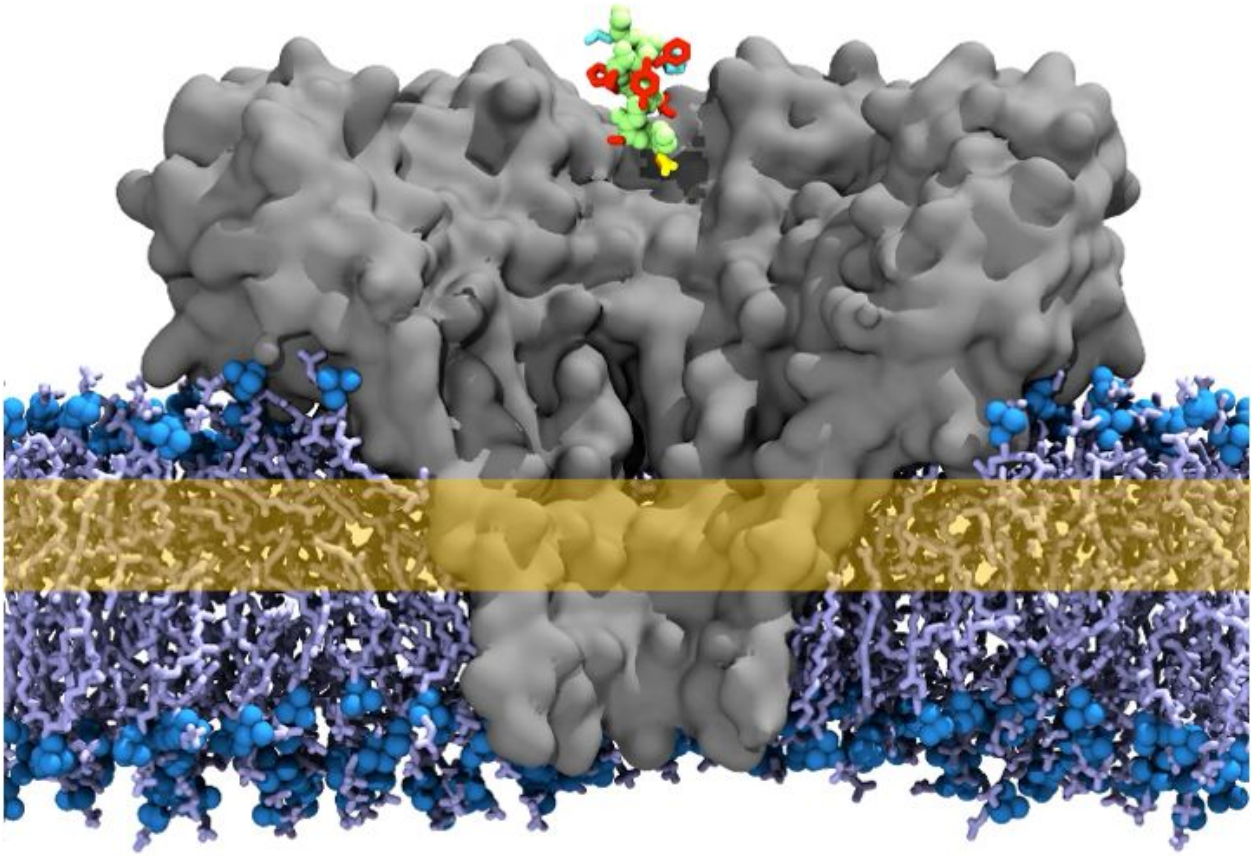

Supplementary Movie 1: SMD simulation of Ang-I peptide translocation through FraC-Wt-T1 pore. The movie shows an 80 ns MD trajectory where an Ang-I peptide (DRVYIHPFHL) was driven through the FraC WT type-I pore using the SMD protocol. The pore is shown as a grey, cutaway molecular surface; the DPhPC lipid bilayer is shown in cyan (head groups) and blue (lipid tails); the backbone of the peptide is shown in green; from the bottom, the first residue (D) is shown in orange, the second residue (R) is shown in yellow, the next 5 residues (VYIHPF) are shown in red, followed by the last two residues (HL) in cyan. The sensing region defined in Fig. 6D is shown as a translucent yellow region.

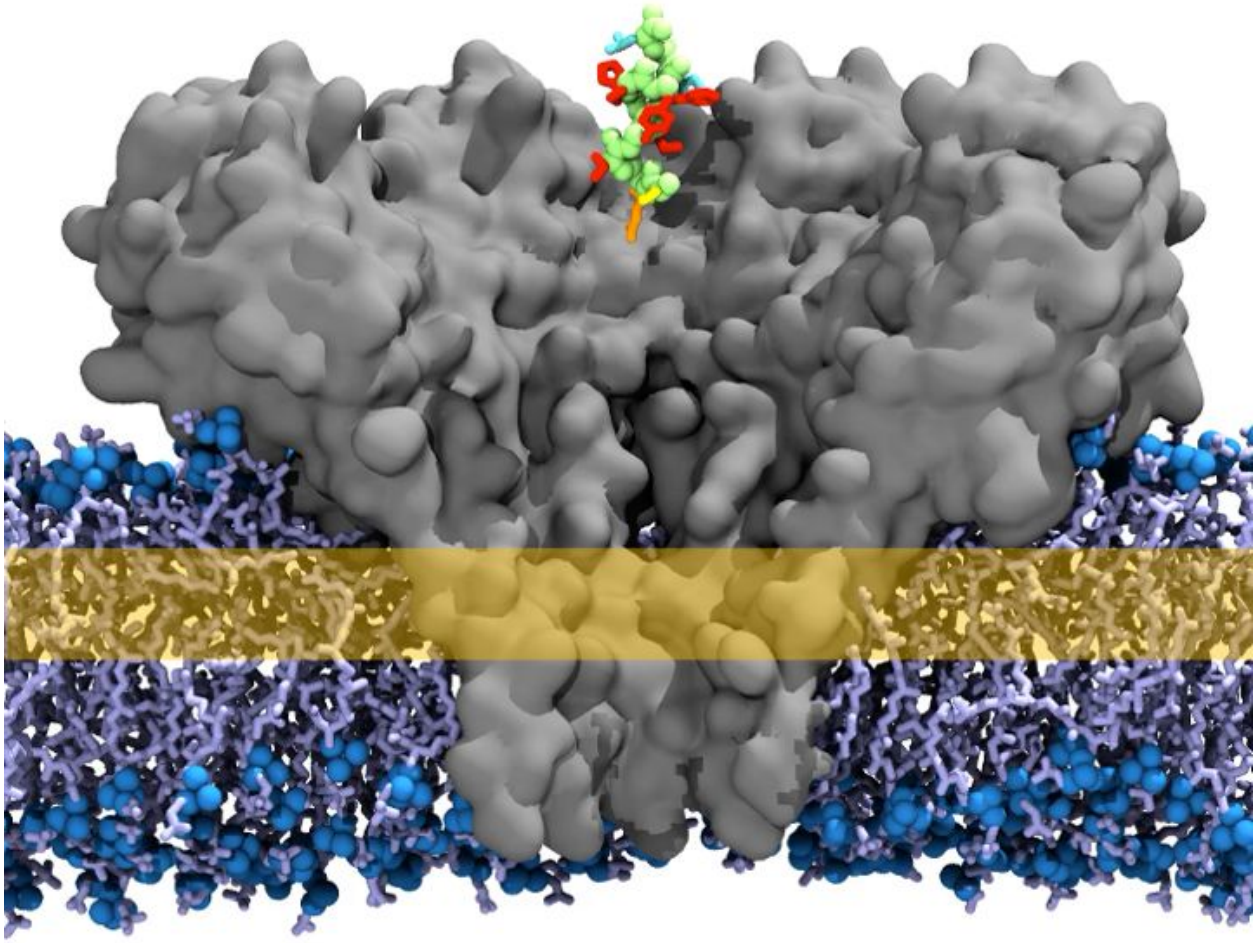

Supplementary Movie 2: SMD simulation of Ang-I peptide translocation through FraC-G13F-T1 pore. The movie shows an 80 ns MD trajectory where an Ang-I peptide (DRVYIHPFHL) was driven through the FraC G13F type-I pore using the SMD protocol. The pore is shown as a grey, cutaway molecular surface; the DPhPC lipid bilayer is shown in cyan (head groups) and blue (lipid tails); the backbone of the peptide is shown in green; from the bottom, the first residue (D) is shown in orange, the second residue (R) is shown in yellow, the next 5 residues (VYIHPF) are shown in red, followed by the last two residues (HL) in cyan. The sensing region defined in Fig. 6E is shown as a translucent yellow region.

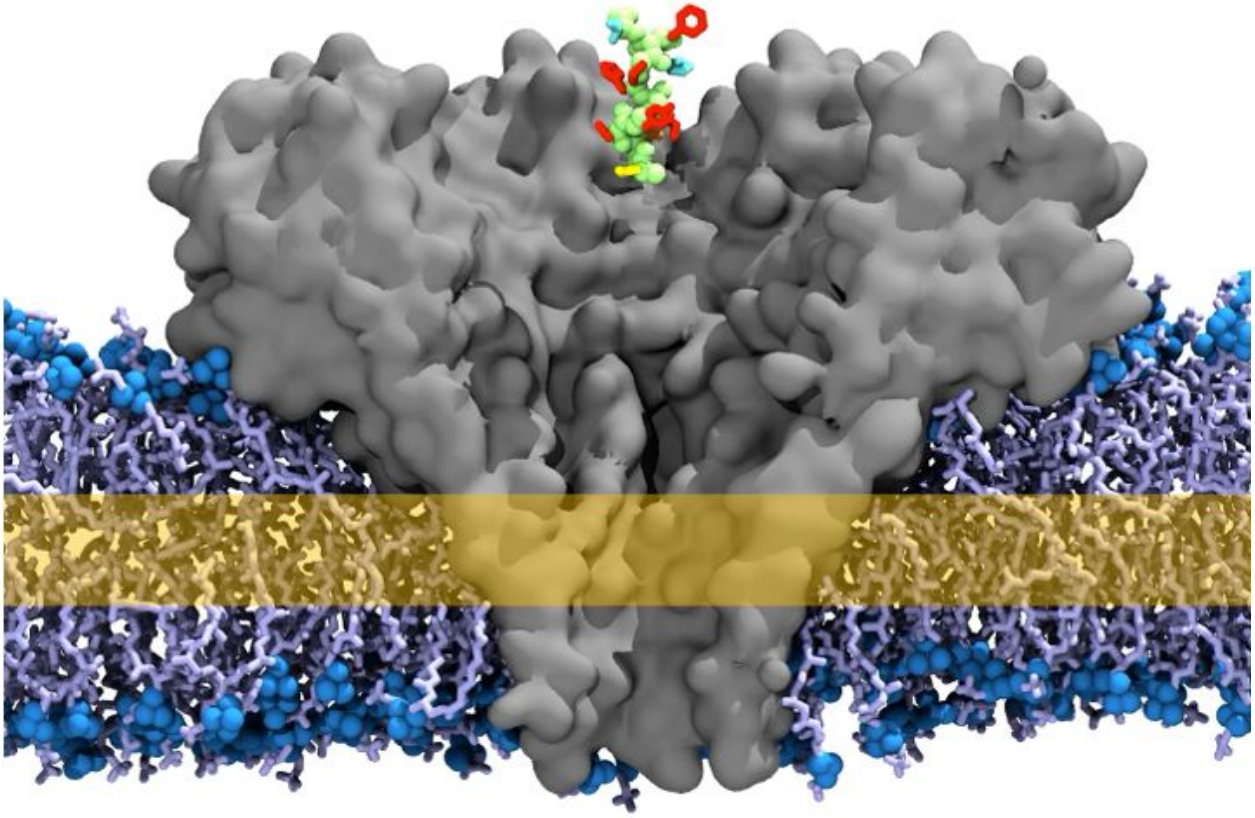

Supplementary Movie 3: SMD simulation of Ang-I peptide translocation through FraC-Wt-T2 pore. The movie shows an 80 ns MD trajectory where an Ang-I peptide (DRVYIHPFHL) was driven through the FraC WT type-II pore using the SMD protocol. The pore is shown as a grey, cutaway molecular surface; the DPhPC lipid bilayer is shown in cyan (head groups) and blue (lipid tails); the backbone of the peptide is shown in green; from the bottom, the first residue (D) is shown in orange, the second residue (R) is shown in yellow, the next 5 residues (VYIHPF) are shown in red, followed by the last two residues (HL) in cyan. The sensing region defined in Fig. 6F is shown as a translucent yellow region.